Network Formation in Dilute Amylose and Amylopectin Studied by TEM

ARTICLE *in* MACROMOLECULES · AUGUST 2000

Impact Factor: 5.8 · DOI: 10.1021/ma000242j

3 AUTHORS, INCLUDING:

Jean-Luc Putaux
French National Centre for Scientific Research
178 PUBLICATIONS **5,168** CITATIONS
SEE PROFILE

Henri Chanzy
French National Centre for Scientific Research
69 PUBLICATIONS **4,816** CITATIONS
SEE PROFILE

Network Formation in Dilute Amylose and Amylopectin Studied by TEM

Jean-Luc Putaux,*,† Alain Buléon,‡ and Henri Chanzy†

Centre de Recherches sur les Macromolécules Végétales—CNRS,§ BP 53, F-38041 Grenoble Cedex 9, France, and Laboratoire de Physicochimie des Macromolécules, INRA, BP 71627, F-44316 Nantes Cedex, France

Received February 9, 2000; Revised Manuscript Received May 31, 2000

ABSTRACT: The retrogradation, or reprecipitation, of dilute amylose and amylopectin aqueous solutions was investigated by transmission electron microscopy (TEM). Negative staining, shadowing, and cryo-TEM were combined to study the morphology of the molecular assemblies at different stages of precipitation. Amylose fractal-like networks formed within a few days. They are described as clusters of elementary semicrystalline 10−15 nm units, formed by associations of molecules into parallel double helices, linked by amorphous sections containing loosely organized chains. These networks subsequently condensed, yielding thick aggregates. Amylopectin was found to form similar networks whose branches also had a 10−15 nm lateral width. The elementary units are thought to be clusters of nanocrystals formed by association of the short side branches of the molecule into parallel double helices. As the amylopectin networks were stable in solution at this concentration during several months and did not undergo any further aggregation, the branched configuration of the molecule is believed to hinder the long-scale rearrangement of the crystallites.

Introduction

The gelation of starch as well as that of its two major components, namely amylose and amylopectin, has been extensively studied,[1−10] but the mechanisms involved in the aggregation of these macromolecules and the fine structure of the resulting networks are not well understood.

Amylose is essentially a linear polysaccharide composed of α(1→4)-linked D-glucosyl units while amylopectin consists of short amylose segments highly branched through α(1→6) linkages.[11] The shape and dimensions of these macromolecules in solution, especially amylose, have mainly been studied using light scattering.[12−14] The global conformation of amylose in dilute aqueous solution has proved to be a random coil in pure water[12] and a more or less extended random coil in KOH[13] or DMSO.[12] Aqueous solutions of amylose or amylopectin are known to be unstable. Upon cooling and aging, they gel, precipitate, and/or crystallize, depending on the sample concentration and its molecular weight. These phenomena—specifically named "retrogradation" for starch products—have been described in a number of reports dealing with starch and amylose, using different techniques: rheology,[6,15] small- and wide-angle X-ray scattering,[16−21] ^{13}C solid-state NMR,[22] small-angle neutron scattering (SANS),[23] infrared spectroscopy,[24] Raman spectroscopy,[25,26] differential scanning calorimetry,[27] and electron microscopy.[28−34] More recently, simulations of the gelation/crystallization of amylose have also been performed by fitting X-ray scattering curves.[35]

The primary mechanism for amylose gelation has been attributed to a change from a random coil state to a phase-separated gel-like network with polymer-rich and polymer-deficient regions.[6] Amylose and amylopectin gels are usually crystalline and yield a classical B-type pattern when probed by X-ray diffraction. The mechanisms involved in the crystallization of B-type amylose and amylopectin in dilute solutions are not well-known. The B-type crystal consists of a hexagonal packing of double helices with the $P6_1$ space group.[36,37] The crystallization step has been proposed to occur either after phase separation over a longer time scale[18] or during phase separation by aggregation of double helices, formed prior to phase separation by molecular entanglement.[38,39] Up to now, the different steps involved in precipitation of amylose could not be directly evidenced, and many questions about phase separation, aggregation, gelation, and crystallization have remained unanswered. The lack of information is even greater for amylopectin gels which have been much less studied.

Over the years, a number of reports have presented images of polymers visualized by transmission electron microscopy (TEM), but most classical techniques that were used such as staining and shadowing have required a drying of the sample, which may lead to an artifactual aggregation.[4,35] Cryo-TEM techniques have been developed to yield direct images of the polysaccharide molecules in suspension without drying or staining artifacts, as the molecules are embedded in a preserving layer of amorphous ice.[40−44] With such a technique, it has indeed become possible to visualize the shape and the dimensions of polysaccharides during aggregation and gelation in dilute solutions at different steps of retrogradation, from the more or less isolated molecules (random coils) through evolution of the crystalline network, if any.[45]

In the present work, cryo-TEM as well as negative staining and shadowing techniques have been used to characterize the behavior of dilute amylose and amylopectin aqueous solutions as a function of time. The dimensions and shape of the elementary structures constituting the networks at different steps of aggregation and crystallization were determined and analyzed

† Centre de Recherches sur les Macromolécules Végétales.
‡ Laboratoire de Physicochimie des Macromolécules.
§ Affiliated with the Joseph Fourier University of Grenoble.
* Corresponding author: Tel +33 476037604; Fax +33 476547203; E-mail putaux@cermav.cnrs.fr.

10.1021/ma000242j CCC: $19.00
Published on Web 08/03/2000

in terms of known structural features of amylose and amylopectin. Our data were compared to those of other authors who used different techniques of characterization.

Materials and Methods

Amylose and Amylopectin Solutions. Commercial Avebe (The Netherlands) amylose powder was used to prepare 0.1% (w/v) solutions. The powder was diluted in water and subjected to nitrogen bubbling for 15 min to remove dissolved oxygen and prevent oxidation during the subsequent high-temperature treatment. Two different methods were then used to solubilize amylose. Some solutions were poured into a plastic autoclave and heated in a microwave oven at 950 W for 35 s. Other solutions were sealed in glass tubes, inserted into a steel autoclave, immersed into an oil bath, and heated at 155 °C for 15 min. Both solutions were then allowed to cool to room temperature.

Amylopectin was extracted from waxy maize (Waxilys, Roquette, France), which contains about 99% amylopectin and about 1% lipids. This lipidic fraction was removed by dissolution of the product in 95% DMSO and reprecipitation in ethanol. A 0.1% (w/v) aqueous solution was prepared using a sealed glass tube heated in an oil bath at a temperature of 50 °C.

After cooling to room temperature, all solutions were filtered with 0.2 μm Millipore filters and stored at 6 °C in a refrigerator. They were regularly shaken in order to minimize the effect of sedimentation.

Transmission Electron Microscopy. A 40 μL aliquot of each suspension was deposited on glow-discharged carbon-coated grids. The liquid in excess was blotted away with filter paper, and 40 μL of 2% uranyl acetate negative stain was added prior to drying. After 1 min, the stain in excess was blotted, and the thin remaining liquid film was allowed to dry. Additionally, some unstained dry specimens were shadowed using W/Ta. The samples were observed in low dose conditions, at a magnification of 20 000×, using a Philips CM200 "Cryo" microscope operated at 80 kV. Images were recorded on Agfa Scientia films.

As described elsewhere,[43] thin vitrified films of the suspensions were prepared for cryo-TEM using a Leica EM CPC fast-freezing device. A drop of a 0.1% (w/v) suspension was deposited on commercial "lacey" NetMesh carbon films (Pelco). The excess liquid was blotted with filter paper. Before evaporation of the remaining fluid, the grids were quench-frozen into liquefied ethane cooled to −171 °C with liquid nitrogen. The specimens were then transferred into a Gatan 626 cryoholder kept at −180 °C with liquid nitrogen. They were observed under low dose conditions at 80 kV and a magnification of 20 000×. Micrographs were recorded with an underfocus of 1−3 μm.

X-ray Diffraction. After centrifugation, samples were sealed between two aluminum foils in order to prevent any significant change in water content during the measurement. Diffraction diagrams were recorded using a transmission technique with a XRG 3000 X-ray generator (Inel Orléans, France) operating at 40 kV and 30 mA. The Cu Kα_1 radiation ($\lambda = 0.154\ 05$ nm) was selected using a quartz monochromator. A curved position-sensitive detector (Inel CPS120) was used to monitor the diffracted intensities using an exposure time of 6 h.

Results

Amylose. A specimen for TEM was prepared from a heat-treated 0.1% (w/v) suspension just after cooling to room temperature. As seen in Figure 1a, polydisperse objects were observed. Since they are revealed by the outer cast of heavy atoms from uranyl acetate, they appear clear on a dark background. The smallest objects look like spheroidal particles with a diameter of 10−20 nm while the largest ones exhibit a wormlike shape with lengths ranging from 50 to 100 nm.

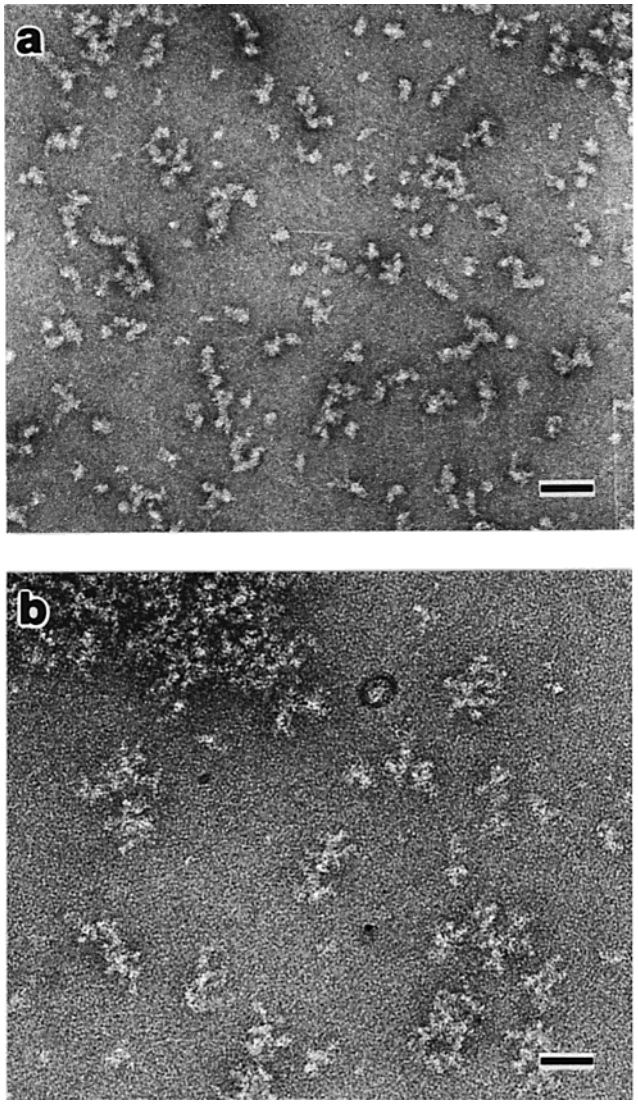

Figure 1. A 0.1% (w/v) aqueous amylose suspension observed: (a) a few minutes after solubilization and cooling to room temperature; (b) after a few hours at room temperature. Both specimens were negatively stained with 2% uranyl acetate (scale bars: 50 nm).

As shown in Figure 1b, after a few hours, the wormlike objects became associated with form larger aggregates whose building units retained the 10−20 nm lateral size. After 1 week at 6 °C, the suspension contained aggregates with sizes up to a few micrometers. A typical negatively stained aggregate is shown in Figure 2a. It appears as a fractal-like network with a rather loose organization of granular branches.

To prevent the drying artifacts, cryo-TEM was also used. Amylose was fast-frozen in suspension so that its hydration and 3D shape were maintained. In Figure 2b, the amylose network can be seen embedded in vitreous ice. The ramifications appear darker than the surrounding medium. As the micrograph was recorded in bright field mode, where only the transmitted electrons were allowed to form the image, the contrast depends on thickness and density (diffusion), as well as crystallinity (diffraction). In addition, a contribution to the contrast is made by the Fresnel effect produced by the defocus of the TEM objective lens which creates fringes at the edges of the embedded objects. The networks are darker

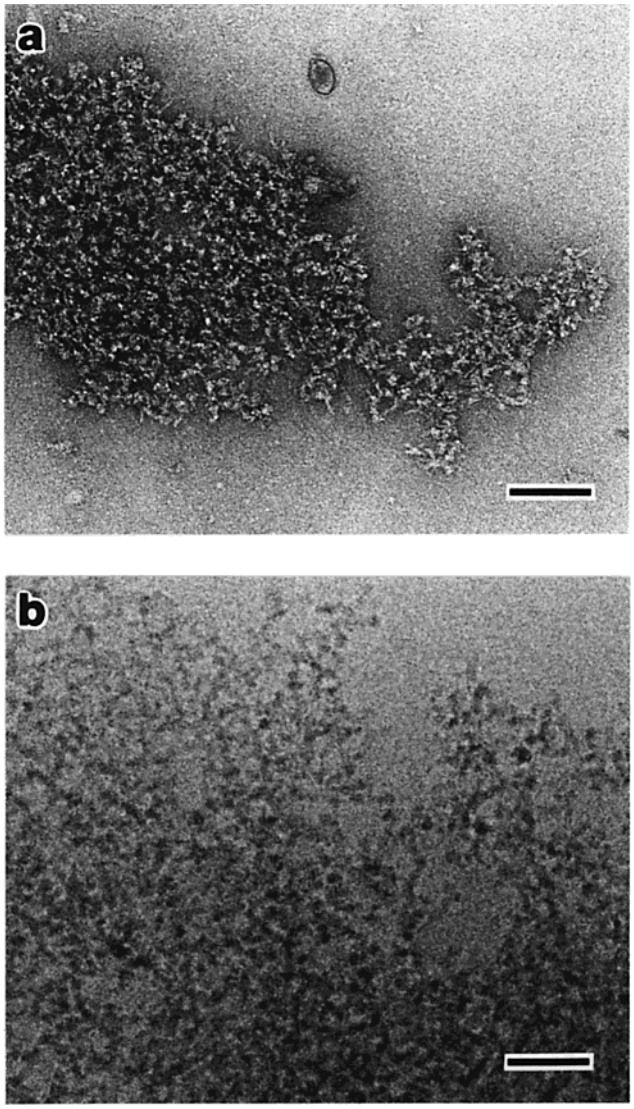

Figure 2. Amylose networks in a 0.1% (w/v) solution after 1 week at 6 °C: (a**)** negative staining; (b**)** bright field cryo-TEM in vitreous ice (scale bars: 100 nm).

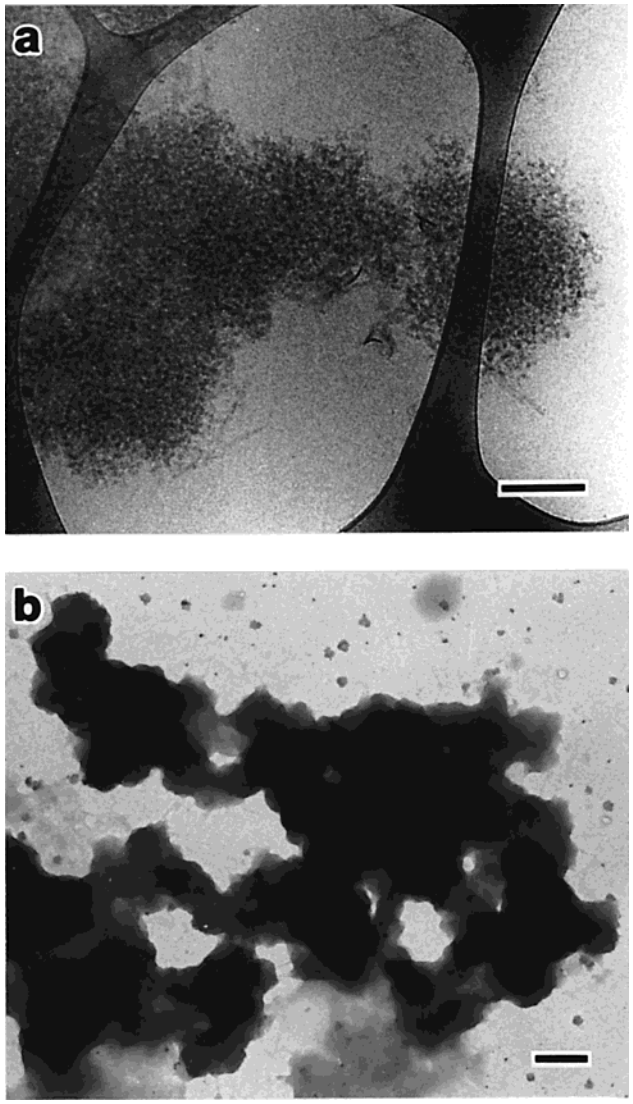

Figure 3. (a**)** Amylose networks in a 0.1% (w/v) solution observed by cryo-TEM in bright field mode after 6 weeks at 6 °C (scale bar: 200 nm). (b**)** Unstained amylose aggregates observed in bright field mode after 6 months at 6 °C (scale bar: 500 nm)

than the embedding ice partly because of the higher density of amylose compared to that of water. In addition, although the contrast along the branches generally appears regular, some local changes can sometimes be observed which might be due to local variations in thickness or crystallinity.

As seen in Figure 3a, after 6 weeks, the networks heterogeneously condensed to form smaller cotton-ball-like aggregates with a diameter of 300−500 nm. As the image was recorded in vitreous ice, the aggregates did not undergo any dehydration due to drying. However, their 3D shape cannot be known with certainty as, when dispersed in a thin liquid water film prior to freezing, the objects are submitted to strong surface tensions which might modify their shape. The thickness of commonly used vitreous ice film is generally estimated to be between 50 and 150 nm. A gel-like water-rich aggregate with an initial diameter larger than 150 nm certainly flattens during the thin film formation. Consequently, the lateral extension measured from the images is artifactual. However, while the aggregate can be considered as distorted to some extent, it certainly retains some 3D features within the 50−150 nm thickness of the embedding medium.

After several months, thick aggregates developed, as seen in Figure 3b, which appear composed of roughly polygonal blocks with a diameter of 200−300 nm. No substructure could be detected.

Amylopectin. After cooling the solution down to room temperature, polydisperse wormlike objects were observed (Figure 4). At first sight and using negative stain, they did not look much different from those observed in amylose solutions except that their branched character was more pronounced. Their length was 40−70 nm and their lateral width 10−15 nm. Within a few days, these objects interacted to form small aggregates, and after a few weeks, the solution contained larger networks.

After 8 months, fractal-like networks such as the one shown in Figure 5a were observed. While amylose networks looked rather dense and intricate (Figure 3a), those of amylopectin exhibited a looser organization. One can recognize branching points and wormlike segments with a length of 30−70 nm and a lateral width still ranging from 10 to 15 nm together with an overall granular aspect. As more clearly seen in Figure 5b, recorded at a higher magnification, the branches have

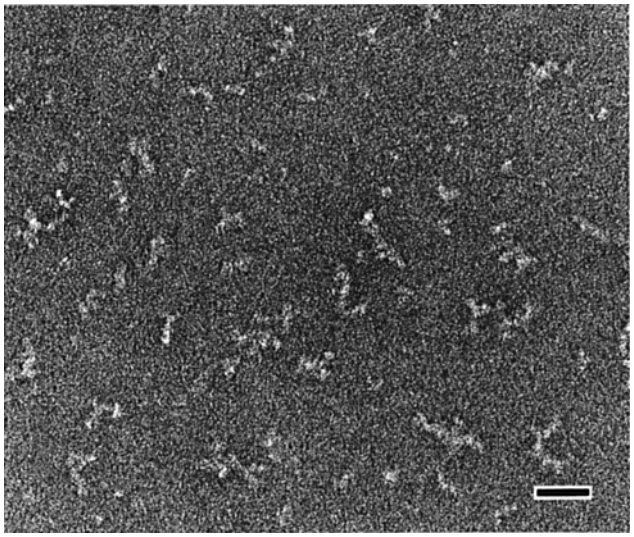

Figure 4. 0.1% (w/v) amylopectin aqueous suspension observed a few minutes after solubilization and cooling to room temperature. The specimen was negatively stained with 2% uranyl acetate (scale bar: 50 nm).

a necklace-like substructure. A similar network observed by cryo-TEM in vitreous ice is shown in Figure 6a in which the granular substructure is even more clearly revealed. As seen in Figure 6b, when dried and W/Ta-shadowed, the specimen looks like a powder and seems to have lost the wormlike network morphology which was an important feature in negative staining and cryo-TEM micrographs (Figures 5a and 6a, respectively). Nevertheless, in the three types of images, the specimen appears to be formed by smaller units. We did not observe any further evolution of these networks with time. Conversely to those formed in retrograded amylose, they did not condense to form thicker aggregates.

Discussion

Comparison of the Various Imaging Techniques. The different preparation techniques of TEM specimens are known to introduce various artifacts which may modify the shape and size of the objects. Negative staining takes advantage of the amplitude contrast created by a cast of heavy atoms surrounding the objects after drying. When added prior to complete drying, the stain is believed to have a sustaining effect that partly counterbalances the collapse due to drying and adsorption on the supporting film. Comparing the micrographs in Figures 5a and 6b, it is clear that, despite the drying, the stain preserved the continuity of the network branches whereas when dried and shadowed, the corresponding network looks more like a powder and it is difficult to recognize any branching pattern.

Negative staining remains a fast and convenient technique to get a general idea of the network morphology with good contrast. However, it is difficult to precisely know the effect of the stain on the configuration of the molecular assembly. Moreover, as amylose networks are known to contain water, one can expect them to undergo some flattening and shrinkage when dried on carbon films. Such a drying might induce some artifactual aggregation and explain why the network appeared more condensed in negatively stained amylose images than in the corresponding cryo-TEM micrographs. The drying effect also explains why no significant differences were observed between images of 1 and

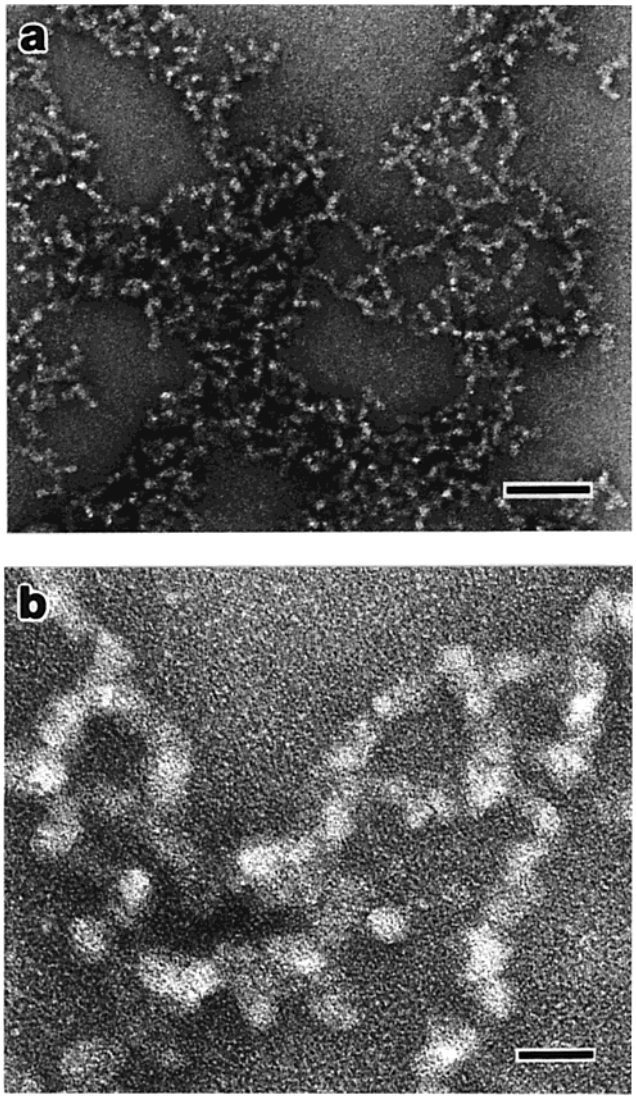

Figure 5. (a**)** Negatively stained amylopectin network in a 0.1% (w/v) solution after 8 months at 6 °C (scale bar: 100 nm). (b**)** Detail of a network branch observed at a higher resolution (scale bar: 20 nm).

6 week old networks. On the contrary, in cryo-TEM images, a rather loose network and a more strongly aggregated configuration were observed after 1 week (Figures 2b) and 6 weeks (Figure 3a), respectively. At a more local scale (i.e., 10−20 nm), negative staining images suffered from a large variability most probably due to the drying conditions, stain concentration, and specimen/stain interactions. The contrast observed in cryo-TEM pictures was more reproducible as was the shape of the objects.

From a more quantitative point of view, the accuracy of the measurements from infocus cryo-TEM images was limited by two factors. On one hand, the interface between the molecules and the vitreous ice was not very clear, perhaps because of the hydration of the structures but also because of the blurring effect of inelastic electron scattering by ice. On the other hand, considering the low intrinsic contrast of the networks in ice, it was generally necessary to record images with a strong underfocus in order to get better contrast. This enhanced the Fresnel effect which created fringes around the objects and, at the same time, decreased the precision of the size measurements. These limitations are inherent to the low density and small size of the

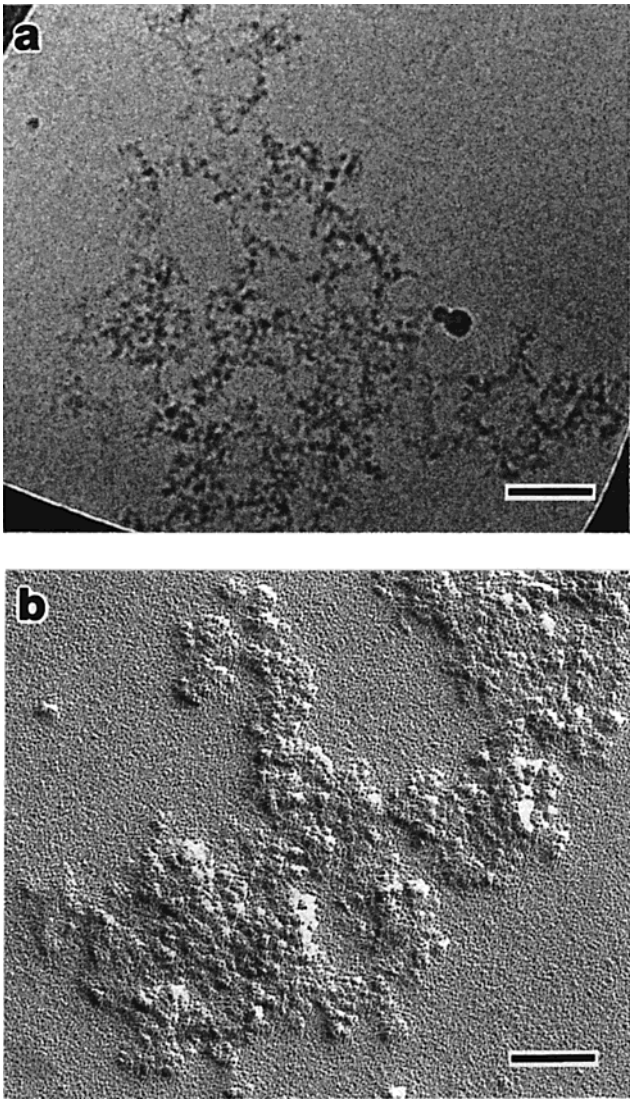

Figure 6. Amylopectin networks in a 0.1% (w/v) solution after 8 months at 6 °C: **(**a**)** cryo-TEM in vitreous ice (bright field); (b**)** shadowing with W/Ta (scale bars: 100 nm).

objects which prevent achieving the high level of accuracy usually obtained for similar observations on viruses[40] or dendrimers.[42]

Amylose Retrogradation. We could not successfully observe early molecular configurations by cryo-TEM, and only images of negatively stained specimens could be recorded (Figure 1a). We assumed that the level of organization in the objects was not high enough to give rise to sufficient contrast and that the high inelastic electron scattering from the embedding ice was to high to allow a clear observation of such small objects. The wormlike configurations presented in Figure 1a may be more clearly delimited due to an effect of drying and/or negative staining.

The amylose molecules are known to be semiflexible in aqueous solutions where they adopts a spheroidal shape. Upon cooling, intra- and intermolecular interactions happen in solution. Considering the degree of polymerization (DP) of individual Avebe amylose molecules (1250) and an estimate of the volume of the smallest objects observed at the early stage of retrogradation (Figure 1a), we can assume that the basic units are made of one to a few (<5) molecules in a coiled or partly organized conformation. Larger wormlike objects

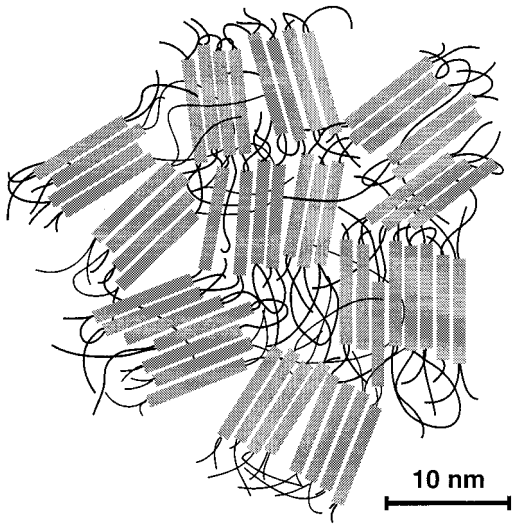

Figure 7. Schematic 2D model of a part of a retrograded amylose network. The gray rods correspond to double helices.

would then correspond to the association of those smaller particles by weak noncovalent interactions (hydrogen-bonding and hydrophobic interactions).[5] The random conformation of the coiled amylose molecules implies that the double helices may form by both inter- and intramolecular interactions. As a consequence, both parallel- and antiparallel-stranded double helices are likely to occur. Even though the parallel-stranded model is preferred, Müller et al.[35] have shown in their simulations that the energy associated with parallel- and antiparallel-stranded double helices are close.

Then, the helices interact and form B-type semicrystalline units which randomly aggregate into networks. These units are separated by amorphous zones that contain more loosely organized chains (Figure 7). This model is quite similar to that presented by Jane and Robyt.[2] The next step of retrogradation is the condensation of the water-rich networks into dense semicrystalline aggregates. This process involves an increase of the macromolecule to macromolecule interactions at the expense of the macromolecule to solvent ones. It has to be noted that, because of the random nature of the associations as well as the restrained mobility due to both molecular weight and storage temperature, a high crystallinity cannot be achieved.

From TEM images only, it is not possible to know exactly when the basic units can be considered crystalline, although they exhibit a certain amount of diffraction contrast in the cryo-TEM micrographs recorded in bright field mode (Figure 2b). However, X-ray diffraction experiments contributed some interesting information, as shown in Figure 8. A pattern recorded from a 3 day old solution exhibits some weak and broad peaks which can be assigned to characteristic reflections of a B-type phase. This proves that crystallinity has started to develop early in the process. The pattern recorded after 1 month shows that the B character gets more and more pronounced with aging. The crystallinity of B-type starch strongly depends on water content. Because of the very small volume of material that was analyzed, this factor could not be monitored with precision, and the comparison of both diagrams has to be done with care. While water subtraction and smoothing procedures were used on the diagram from the 3 day old sample to improve the low signal-to-noise ratio, the amount of

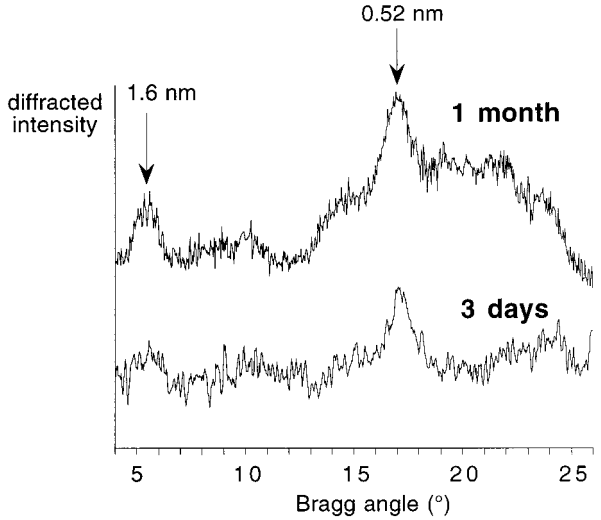

Figure 8. X-ray diffraction patterns recorded on 0.1% (w/v) amylose solutions. (a**)** After 3 days. To improve the signal-to-noise ratio, the scattering diagram of pure water was subtracted, and a smoothing procedure was applied. (b**)** After 1 month. Characteristic reflections from B amylose are indicated.

product aggregated after 1 month was sufficient to get a clear diffraction diagram.

It is interesting to compare the data obtained by TEM with those collected using other techniques. In the early stages of retrogradation as well as for larger networks, we observed wormlike molecular assemblies with a characteristic lateral size of 10−15 nm. Studying 2−8% (w/v) retrograded amylose solutions by SANS, Vallêra et al. observed a fractal structure with basic aggregating units with a mean diameter of ∼20 or 13.5 nm depending on whether they were assimilated to spheres or cylinders, respectively.[23] This result was relatively independent of the concentration. Observing replicas obtained from cryo-fractured, frozen-etched, and rotary-shadowed samples of 2−8% (w/v) amylose solutions, Leloup et al. observed filamentous structures with a diameter between 10 and 20 nm.[31] Harada et al. investigated dilute solutions prepared from starch or amylose from different origins.[30] Their TEM micrographs showed negatively stained branched networks very similar to the ones presented in our work. From these pictures as well as ours, the lateral branch size was measured to be 10−15 nm. It appears that our measurements are in agreement with the characteristic dimension common to the reports of all these authors[23,30,31] even though they dealt with more concentrated solutions.

Amylopectin Retrogradation. Individual amylopectin molecules are different from amylose in structure and size so the objects observed in the early stage of retrogradation are expected to have a different morphology. As for amylose, it has not been possible to record images of these molecular configurations by cryo-TEM. Comparing the pictures in Figures 1a and 4, both from negatively stained samples, little can be said about morphological differences. A thorough study of this early stage was carried out by Fishman et al.[33] Some specific features rapidly appeared as more extended networks started to develop. Although the images presented in Figure 5 were obtained from 8 month old solutions, similar networks were observed within the first few days of retrogradation.

As shown in Figure 5b, the amylopectin network branches have a necklace-like morphology. Referring to

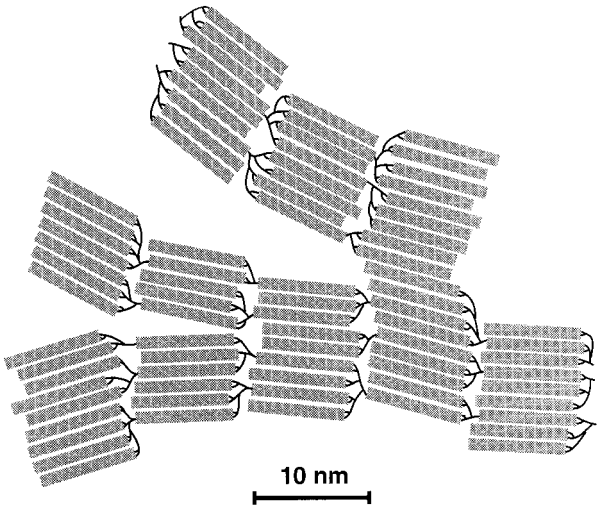

Figure 9. Schematic 2D model of a part of a retrograded amylopectin network. The gray rods correspond to double helices.

the widely accepted "cluster model",[20] we assumed that the necklace "pearls" were formed by the lateral packing of double helices whose axes were parallel to the direction of a network branch. Measurements performed by different authors on native starch granules would indicate that the thickness of such a unit (as measured along the *c* axis) would be 9−10 nm[21] and the lateral width 14−15 nm.[46] This is in good agreement with our observations. Taking into account the crystallographic model of B amylose and the interhelical distance of 1.6 nm, units with a perfect hexagonal packing would be made of about 100 double helices.[35] For cereals, amylopectin molecules are known to mainly contain short (DP 15) and long (DP 45) chains with a short/long ratio of 8 to 10. We can thus assume that while the short side chains are involved in the formation of double helices, about 10 chains with DP 45 will be common to two basic units (Figure 9).

The first stage of amylopectin retrogradation involves a majority of intramolecular interactions, as the primary structure of amylopectin favors the formation of double helices by intertwinning of the small lateral branches of the molecule.[24−26] Parallel-stranded helices form and pack up into B-type crystallites. Then, the basic clusters of crystallites, linked by ill-organized zones containing α(1→ 6) junctions, cross-link to form fractal-like networks (Figure 9).

Some steps of retrogradation, such as chain interactions, formation of double helices, crystallization, and network formation, are common to amylose and amylopectin. However, our results have shown that months old amylopectin networks had a morphology which was quite similar to that of 1 week old amylose networks. While the retrogradation of dilute amylose solutions is a process involving a continuous condensation of the networks over several months, the evolution of amylopectin is stopped at an earlier stage. As previously described, the structural features of the clusters formed during the first steps of precipitation and the shortness of intercrystalline segments impart a strongly restrained mobility to the branches. In addition, the solubility of amylopectin in water is known to be higher than that of amylose. This may be an important factor to consider.

Conclusion

For the first time, cryo-TEM has been used to characterize the morphology of amylose and amylopectin networks at various steps of precipitation in dilute aqueous solutions. Although cryo-TEM images are snapshots of the molecular assemblies frozen in solution, the technique proved useful to study some aspects of the long-term retrogradation kinetics. Both types of molecules rapidly rearrange at the local scale to form basic units whose crystallinity is not known with precision. Amylose retrogradation appears as a continuous process involving first a clustering of the semicrystalline units into branched networks, followed by a slow condensation of these networks into thick semicrystalline aggregates. Amylopectin seems to follow a similar pathway in the early stages of retrogradation, although the basic units are clusters of crystallites formed by association of the side branches of the molecules. The molecular assemblies appear to be stable in a loose network configuration and do not evolve toward any further aggregated state. It is thus believed that the branching scheme of the native amylopectin molecule somehow hinders the aggregation process.

Cryo-TEM may be useful to get additional information regarding the crystallinity of the networks as well as the orientation of the molecules with respect to the branches. On one hand, electron diffraction patterns recorded in vitreous ice might allow assessement of the crystallinity of retrograded networks as well as the crystal type. However, as the crystallinity appears to be rather low, the signal might be obscured by the high inelastic electron scattering of the embedding ice. In that case, the use of an in-line energy filter to remove the contribution of the inelastic scattering in the diffraction pattern would certainly help. Second, high-resolution lattice images of the networks in vitreous ice may reveal the 1.6 nm spacing that is characteristic from B-amylose. From an instrumental point of view, imaging such spacing should not be a problem as commercial 200 kV microscopes typically reach resolutions of 0.2 nm. Nevertheless, the molecular order in such small crystallites might not be sufficient to get a clear image of the 1.6 nm interhelical spacing. In addition, the inelastic electron scattering will certainly hinder the amplitude of the corresponding weak signal.

Using TEM to obtain lattice information from weakly organized retrograded amylose and amylopectin networks is a significant challenge, but hopefully, the use of microscopes combining the resources of energy filtering and cryotechniques will help to overcome some of the difficulties.

References and Notes

(1) Huseman, E.; Pfannemüller, B. P.; Burchard, W. *Makromol. Chem.* **1963**, *59*, 1−15.

(2) Jane, J. L.; Robyt, J. F. *Carbohydr. Res.* **1984**, *132*, 105−118.

(3) Miles, M. J.; Morris, V. J.; Ring, S. G. *Carbohydr. Res.* **1985**, *135*, 257−269.

(4) Gidley, M. J.; Bulpin, P. *Macromolecules* **1989**, *22*, 341−346.

(5) Gidley, M. J. *Macromolecules* **1989**, *22*, 351−358.

(6) Doublier, J. L.; Choplin, L. *Carbohydr. Res.* **1989**, *193*, 215−226.

(7) Leloup, V. M.; Colonna, P.; Buléon A. *J. Cereal Sci.* **1991**, *13*, 1−13.

(8) German, M. L.; Blumenfeld, A. L.; Guenin, Y. V.; Yuryev, V. P.; Tolstoguzov, V. B. *Carbohydr. Polym.* **1992**, *18*, 27−34.

(9) Ward, K. E. J.; Hoseney, R. C.; Seib, P. A. *Cereal Chem.* **1994**, *71*, 150−155.

(10) Lu, T. J.; Jane, J. L.; Keeling, P. L. *Carbohydr. Polym.* **1997**, *33*, 19−26.

(11) Buléon, A.; Colonna, P.; Planchot, V.; Ball, S. *Int. J. Biol. Macromol.* **1998**, *23*, 85−112.

(12) Nakata, Y.; Kitamura, S.; Takeo, K.; Norisuye, T. *Polym. J.* **1994**, *26*, 1085−1089.

(13) Roger, P.; Tran, V.; Lesec, J.; Colonna, P. *J. Cereal Sci.* **1996**, *24*, 247−262.

(14) Galinsky, G.; Burchard, W. *Macromolecules* **1995**, *28*, 2363−2370.

(15) Clark, A. H.; Gidley, M. J.; Richardson, R. K.; Ross-Murphy, S. B. *Macromolecules* **1989**, *22*, 346−351.

(16) Miles, M. J.; Morris, V. J.; Orford, P. D.; Ring, S. G. *Carbohydr. Res.* **1985**, *135*, 271−281.

(17) Ring, S. G.; Colonna, P.; I'Anson, K. J.; Kalichevsky, T.; Miles, M. J.; Morris, V. J.; Ordorf, P. D. *Carbohydr. Res.* **1987**, *162*, 277−293.

(18) I'Anson, K. J.; Miles, M. J.; Morris, V. J.; Ring, S. G.; Nave, C. *Carbohydr. Polym.* **1988**, *8*, 45−53.

(19) Gernat, C.; Reuther, F.; Damashun, G.; Schierbaum, F. *Macromolecules* **1989**, *22*, 341−346.

(20) Manners, D. J. *Carbohydr. Polym.* **1989**, *11*, 87−112.

(21) Cameron, R. E.; Donald, *A. M. J. Polym. Sci., Part B: Polym. Phys. Ed.* **1993**, *31*, 1197−1203.

(22) Morgan, K. R.; Furneaux, R. H.; Stanley, R. A. *Carbohydr. Res.* **1992**, *235*, 15−22.

(23) Vallêra, A. M.; Cruz, M. M.; Ring, S.; Boué, F. *J. Phys.: Condens. Matter* **1994**, *6*, 311−320.

(24) Goodfellow B. J.; Wilson, R. H. *Biopolymers* **1990**, *30*, 1183−1189.

(25) Bulkin, B. J.; Kwak, K.; Dea, I. C. M. *Carbohydr. Res.* **1987**, *160*, 95−112.

(26) Winter, W. T.; Kwak, Y. T. *Food Hydrocolloids* **1987**, *1*, 461−463.

(27) Paredes-López, O.; Bello-Pérez, L. A.; López, M. G. *Food Chem.* **1994**, *50*, 411−417.

(28) Pfannemüller, B. P.; Bauer-Carnap, A. *Colloid Polym. Sci.* **1977**, *255*, 844−848.

(29) Yamaguchi, M.; Kainuma, K.; French, D. *J. Ultrastruct. Res.* **1979**, *69*, 249−261.

(30) Harada, T.; Kanzawa, Y.; Kanenaga, K.; Koreeda, A.; Harada, A. *Food Struct.* **1991**, *10*, 1−18.

(31) Leloup, V. M.; Colonna, P.; Ring, S. G.; Roberts, K.; Wells, B. *Carbohydr. Polym.* **1992**, *18*, 189−197.

(32) Cameron, R. E.; Durrani, C. M.; Donald, A. M. *Starch/Staerke* **1994**, *46*, 285−287.

(33) Fishman, M. L.; Cooke, P.: White, B.; Damert, W. *Carbohydr. Polym.* **1995**, *26*, 245−253.

(34) Keetels, C. J. A. M.; Oostergetel, G. T.; van Vliet, T. *Carbohydr. Polym.* **1996**, *30*, 61−64.

(35) Müller, J. J.; Gernat, C.; Schulz, W.; Müller, E. C.; Vorwerg, W.; Damaschun, G. *Biopolymers* **1995**, *35*, 271−288.

(36) Wu, H. C. H.; Sarko, A. *Carbohydr. Res.* **1978**, *61*, 7−25.

(37) Imberty, A.; Perez, S. *Biopolymers* **1988**, *27*, 1205−1221.

(38) Hanke, D. E.; Northcote, D. H. *Biopolymers* **1975**, *14*, 1−17.

(39) Hermansson, A. M.; Eriksson, E.; Jordansson, E. *Carbohydr. Polym.* **1991**, *16*, 297−320.

(40) Harris, J. R. In *Negative Staining and Cryoelectron Microscopy: the Thin Films Techniques*; Bios Scientific Publishers: Oxford, UK, 1997.

(41) Sugiyama, J.; Rochas, C.; Turquois, T.; Taravel, F.; Chanzy, H. *Carbohydr. Polym.* **1994**, *23*, 261−264.

(42) Jackson, C. L.; Chanzy, H. D.; Booy, F. P.; Drake, B. J.; Tomalia, D. A.; Bauer, B. J.; Amis, E. J. *Macromolecules* **1998**, *31*, 6259−6265.

(43) Putaux, J. L.; Buléon, A.; Borsali, R.; Chanzy, H. *Int. J. Biol. Macromol.* **1999**, *26*, 145−150.

(44) Borgström, J.; Piculell, L.; Viebke, C.; Talmon, Y. *Int. J. Biol. Macromol.* **1996**, *18*, 223−229.

(45) Chronakis, I. S.; Borgström, J.; Piculell, L. *Int. J. Biol. Macromol.* **1999**, *25*, 317−328.

(46) Hizukuri, S.; Nikuni, Z. *Nature* **1957**, *180*, 436−437.

MA000242J